Phononic Crystal Made of Multilayered Ridges on a Substrate for Rayleigh Waves Manipulation

Mourad Oudich, Bahram Djafari-Rouhani, Bernard Bonello, Yan Pennec, Frédéric Sarry

Phononic crystal made of multilayered ridges on a substrate for Rayleigh waves manipulation

M. Oudich[1,2], B. Djafari-Rouhani[3], B. Bonello[4], Y. Pennec[3], F. Sarry[1,2]

[1] CNRS, Institut Jean Lamour, UMR 7198, Vandœuvre-lès-Nancy F-54506, France

[2] Université de Lorraine, Institut Jean Lamour, UMR 7198, Vandœuvre-lès-Nancy 54506, France

[3] Institut d'Electronique, de Micro-électronique et de Nanotechnologie (IEMN–UMR CNRS 8520), Université de Lille1, UFR de Physique, Cité Scientifique, 59652 Villeneuve d'Ascq Cedex, France

[4] Sorbonne Universités, UPMC Université Paris 06, INSP UMR CNRS 7588, 75005 Paris, France

Abstract

We present a phononic crystal to achieve efficient manipulation of surface acoustic waves (SAW). The structure is made of finite phononic micro-ridges arranged periodically in a substrate surface. Each ridge is constructed by staking silicon and tungsten layers so that it behaves as one-dimensional phononic crystal which exhibits band gaps for elastic waves. The band gap allows the existence of resonance modes where the elastic energy is either confined within units in the free end of the ridge or the ones in contact with the substrate. We show that SAW interaction with localized modes in the free surface of the ridge gives rise to sharp attenuation in the SAW transmission while the modes confined within the ridge/ substrate interface cause broad band attenuations of SAW. Furthermore, we demonstrate that the coupling between the two kinds of modes within the band gap gives high SAW transmission amplitude in the form of Fano like peaks with high quality factor. The structure could provide an interesting solution for accurate SAW control for sensing application for instance.

Introduction

There has been numerous works and investigations upon phononic crystals (PCs) as they provide the solution for acoustic and elastic waves control and dispersion manipulation. PCs are constructed by periodic arrangement of solid materials or fluids having different elastic properties which allows the existence of phononic band gaps (BG) where wave propagation is prohibited [1,2]. This property paved the way to consider PC for many applications such as filtering and waveguiding [3-8], sensing [9,10], acoustic wave focusing and lensing [11-14], and topological phononics [15,16]. The rapid progress in phononics led to the appearance of acoustic metamaterials (AM) which demonstrate exceptional properties such as negative effective mass density and/or bulk modulus or compressibility [17-20]. Such behavior led to create new designs of artificial systems capable of remarkable acoustic wave manipulation such as sound insulation [21], sub-wavelength focusing [22,23], and acoustic cloaking [24].

Among the works on PC and AM, structures based on plates attracted more interest as they offer good platforms for elastic wave propagation and integration with low loss and weak mode conversion at wavelength larger than the plate thickness. The first PC systems were constructed by considering periodic distribution of holes or inclusions in the plate [25, 26]. Then, the phononic community quickly turns their interest into elastic pillars deposited on thin plates as they showed promising dispersion properties for Lamb waves. Pennec et al. [7,27] and Wu et al [28,29] proposed a pillar based plate by which they show the arising of local resonance BG (LRBG) created by the resonances of the pillars which couple with the Lamb waves in the band structure. This behavior was experimentally demonstrated by Wu al [28] using a laser ultrasonic technique in an aluminum based pillar plate. In other studies, the acoustic properties of silicone rubber pillars deposited on a rigid plate were investigated [20,30,31]. The structure can produce tunable LRBG at the sonic regime [32], and showed also great performance as a thin sonic insulator with high sound transmission losses [33,34]. Meanwhile, the process of introducing a point or a line defect inside the PC lattice allows the creation of elastic modes in the BG with zero or slow group velocity. Pennec et al. [7, 27] performed elastic waveguiding using a line defect, either by creating a space between two rows of pillars, or changing the pillars height or their material in a row. In another study, the same group proposed a system with hollow pillars where whispering gallery modes can be used to achieve efficient elastic waveguiding [35]. The modes' frequency can be tuned by filling the hollow parts with liquid [36,37]. Wang et al. [38] have shown experimentally similar behavior in a phononic strip. In another study, Wu et al. [29] have demonstrated experimentally the waveguiding feature in a stubbed PC plate using a bent waveguide to change the wave propagation direction in the ultrasonic regime. Very recently, Jin et al. [39] studied the scattering of an incident Lamb wave with a single or a line of pillars and discussed the amplitudes and phases of the monopolar and dipolar waves emitted by these resonators. The Lamb waves confinement and waveguiding were also demonstrated by the pillar based system in the sonic regime [40-42].

Motivated by surface acoustic wave (SAW) manipulation in the ultrasonic regime for sensing and filtering applications, some works dealt with the SAW dispersion by PC. The first systems were constructed by tailoring holes or finite inclusions on a substrate surface [5, 8, 41-46]. Later on, the interest was turned to PC made of micro-pillars deposited in the surface of semi-infinite material for higher dispersion of the SAW. Khelif et al. [47] proposed a two dimensional array of cylindrical pillars by which they demonstrate theoretically the BG opening for SAW by local resonance of the pillars. In the band structure, they show that the BG creation results from the coupling between the resonance modes and the SAW which occurs below the sound cone. This feature is very interesting compared to PC based on inclusions since one can avoid the SAW interaction with bulk acoustic waves (BAW) (occurring above the sound line) which inevitably increases the SAW energy leakage into the bulk substrate. The mechanical

vibrations of pillars were experimentally demonstrated by Achaoui et al. [48] using optical measurements and the arising of LRBG was evidenced through the SAW transmission decay at the resonance frequency. Other works have also detected experimentally the resonance of the pillars in different pillar based PC [49-50]. Yudistira et al. [51] showed the opening of both Bragg BG and LRBG in a hypersonic PC made of pillars, and very recently, Ash et al. [52] were able to detect high SAW attenuation caused by LRBG using a PC system made of pillars in holes (ring holes).

Meanwhile, few works have investigated the possibility of SAW waveguiding. Lethawe et al. [53] proposed a pillar based structure where waveguiding is achieved through a chain of pillars. Very recently, Benchabane et al. [54] demonstrated experimentally the possibility to manipulate the elastic waves in the surface of a substrate using micro-pillars where the elastic energy can be strongly confined at the sub-wavelength scale. For SAW waveguiding achievement by taking advantage of the BG, the classical approach is to introduce a line defect inside the PC to create confined modes within the defect at the BG frequency range. However, this approach makes the defect modes suffer from mode's conversion and become leaky toward the bulk substrate. In the transmission spectrum, the defect modes have large bandwidth to even close the BG, which makes the system not suitable for sensing applications for example.

In this paper, we introduce a PC made of a repetition of phononic ridges built by alternating silicon and tungsten layers (figs.1 (a) and 2(a)). Each ridge is a one-dimensional (1D) PC displaying band gaps where confined modes can be created both in the upper surface of the ridge and its interface with the substrate. We then took advantages of the (1D) PC properties to perform efficient coupling between the SAW and the localized modes in the ridge in order to get high SAW transmission in a very narrow bandwidth. The objective is to get and control high transmitted narrow bands with low radiation into the bulk substrate leading to high QF features. The paper is organized as follows: section II presents the phononic ridge and its dispersion property for elastic waves, and discusses the SAW interaction with the PC made of finite phononic ridges. In section III, we study the SAW transmission through one and three ridge(s) and discuss the coupling mechanisms between the modes of interest.

II. SAW dispersion in the PC system with phononic ridges

We first consider an infinite phononic ridge or plate composed of alternating silicon (Si) and tungsten (W) layers (a periodic beam) in z direction having the same thickness h while both layers have the same width D (fig.1). The system is considered infinite along y direction. When choosing h=3.5 µm and D=6 µm, the band structure of the system displays two BGs denoted BG1 from 243.7 to 387.4 MHz and BG2 from 421.3 to 543 MHz for waves propagation along the z direction (fig.1). The calculations are based on finite element method using Comsol Multiphysics© software.

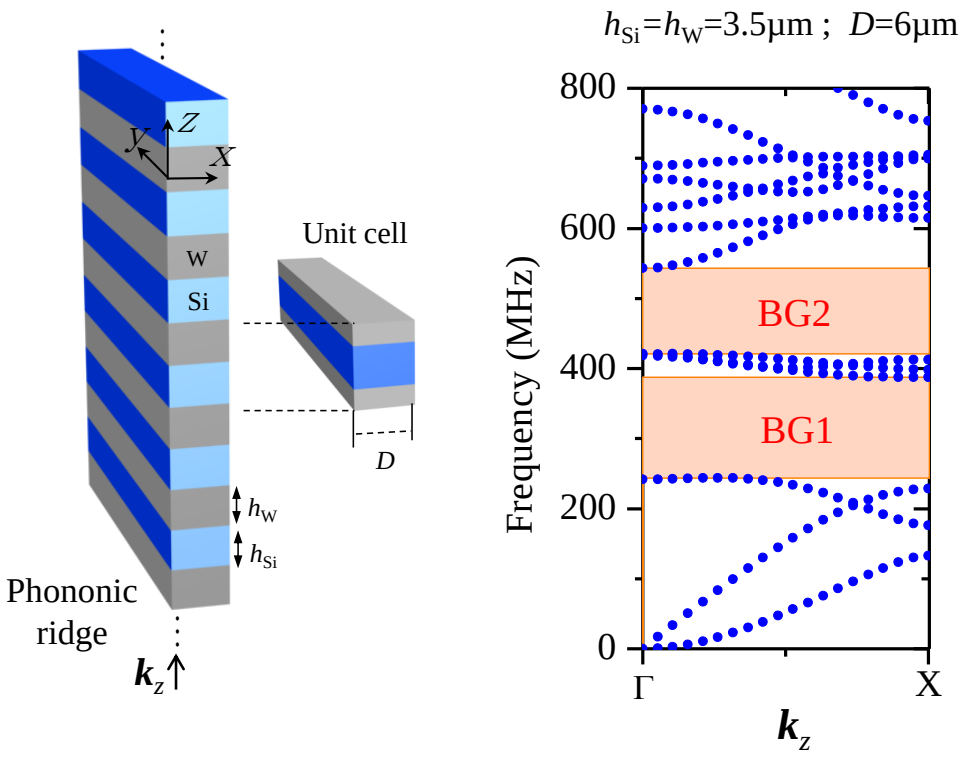

Fig.1. (Left) Phononic ridge made of periodic repetition of silicon and tungsten layers. (Right) the band structure along $\boldsymbol{k}_z$ direction for $h=h_{Si}=h_W=3.5$ µm and $D=6$ µm.

Regarding the SAW dispersion, we built a PC structure using a periodic repetition of finite phononic ridges on the surface of a thick silicon substrate (fig.2(a)). Each ridge is made of 3 Si/W cells ended with a last Si layer on top. The repetition period of the ridges is a=7 µm (the cell period), and the band structure calculation was performed using a unit cell with periodic boundary conditions (PBC) (fig.2(b)). The X' point indicates the Brillouin zone limit π/a in the propagation direction x for SAW. The blue line corresponds to the Si sound line so that the modes located in the cyan shaded region are BAW or leaky surface modes that can radiate into the bulk silicon substrate. The modes located below the sound line are either confined within the surface of the Si substrate or inside the ridge. Some of the modes appear in the orange shaded region which corresponds to the phononic ridge band gap BG1. A mode located in this region cannot propagate into the Si substrate or in the whole ridge. They can only be confined in specific regions of the ridge as we will see below. The other SAW branches outside the BG1 correspond to modes where the elastic energy is spread all along the ridges.

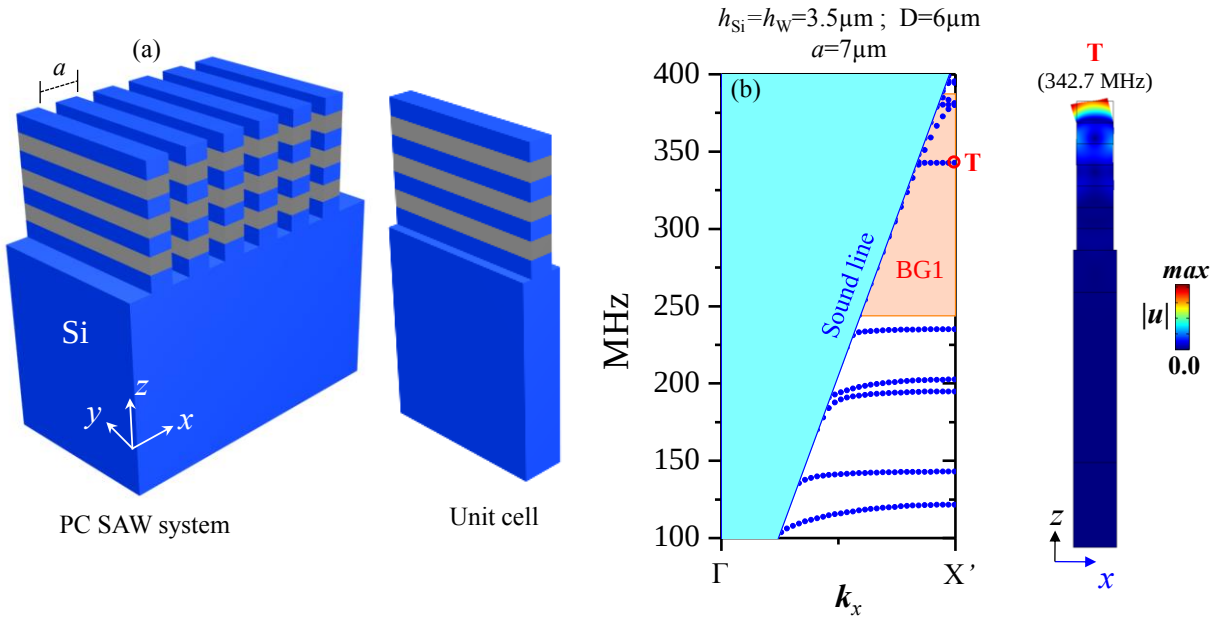

Fig.2. (a) PC structure made of periodic phononic ridges on Si substrate surface along *x* direction. (b) Band structure of the PC system for SAW propagation along *x* direction. The orange shaded region corresponds to the band gap BG1 of the phononic ridge. (Right) Total displacement field amplitude in the unit cell for mode denoted T in the band structure.

From the band structure of fig.2(b), we can depict the presence of one particular flat mode denoted T with zero group velocity at 342.7 MHz inside the BG1 region. We plot in fig.2(b) the total displacement field amplitude with the deformation shape of the mode where we can clearly see its local resonance nature. The resonance is confined within the top of the ridge where the maximum of the displacement field amplitude is located and quickly decays along the first top Si/W layers of the ridge with almost no vibration in the other layers. This behavior is expected since the presence of the stop band BG1 (shaded orange region) of the phononic ridge prohibits the propagation along the whole ridge. Furthermore the mode T displays flexural like mechanical vibration in the top Si/W layers. We notice that the modes located outside the band gaps BG1 region layers are of less interest in this study since there are resonance modes where the mechanical vibration is along the whole ridges.

We now investigate the phononic ridge behavior when changing its geometry. We consider the finite phononic ridge where we change the thickness of the top Si layer denoted h_T in this study (fig.3(a)). In the calculations, we consider a single finite phononic ridge with 3.5 Si/W periods where the bottom Si surface is fixed and the upper surface is kept free. If we choose h_T=5.5 μm for the top Si layer, we can depict three confined modes in the band gap BG1 (fig.3). We plot in fig.3(b) the total displacement field amplitude of these modes to understand their mechanical vibration. The first one denoted T_1 located at 258

MHz has the same mechanical behavior as mode denoted T depicted in the SAW band structure of fig.2(b), where the top Si/W layers display flexural vibration. The second surface localized mode denoted T_2 at 337.5 MHz has a compressional vibrational motion shape in which the top Si/W layers are stretched and compressed along the z direction. The third mode T_3 (373.4 MHz) has flexural mechanical vibration like mode T_1 and can be considered as second order flexural mode. We display in fig.3(c) the frequency dependence on the top Si layer thickness h_T for the three surface modes where the black squares indicate the mode T_1 while the red dots and blue triangles are for resonance modes T_2 and T_3 respectively. The band gap BG1 is indicated by orange shaded region. One can deduce from the result that for each defect mode T_1, T_2 and T_3, the frequency increases when lowering the thickness of the top Si layer. This behavior can be expected knowing that the cavity modes tend to adapt to the defect size so that their wavelength becomes smaller when decreasing h_T.

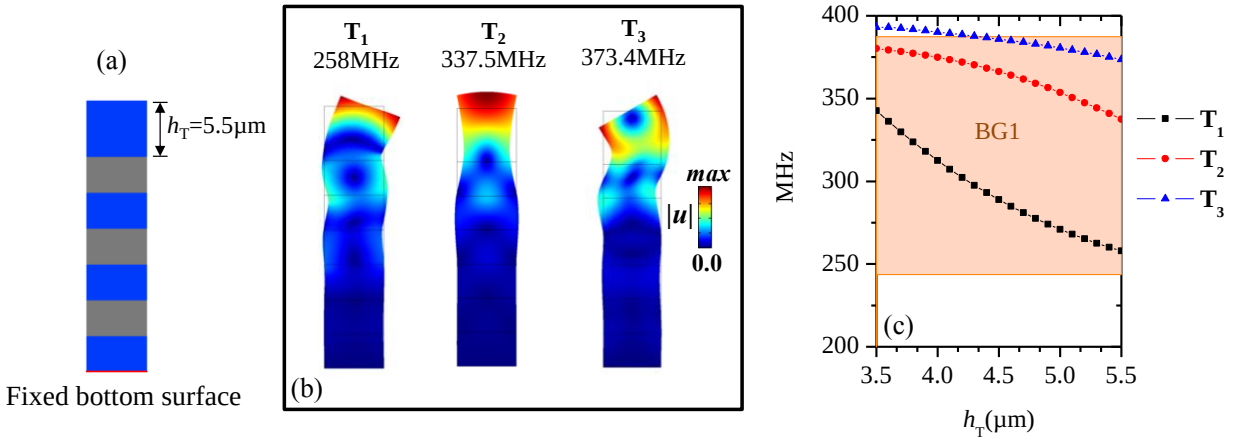

Fig.3. (a) Finite phononic ridge where the structural defect is constructed by changing the thickness h_T of the top Si layer. The bottom surface of the ridge is fixed. (b) Total displacement field amplitude for the resonance modes in the phononic ridge for h_T=5.5 µm. (c) The resonance modes frequency shift as function of h_T.

We then investigate the SAW dispersion with periodic repetition of finite phononic ridges over the Si substrate surface when changing their top Si layer thickness h_T. Fig.4(a) shows the band structure calculation in the case of h_T=5.5 µm. In the frequency range of the band gap BG1, we can depict three local resonance modes with zero group velocity. We also display in fig.4(b) the displacement field amplitude and the deformation profiles of these modes to identify their mechanical behavior. When analyzing the displacement fields, we can clearly identify the flexural resonance modes T_1 and T_3 and the compressional mode T_2, which correspond to the same modes depicted in fig.3(b). Furthermore, the modes T_1, T_2 and T_3 are located at 258, 337.5 and 373.4 MHz which are at the same frequencies as in the

case of isolated ridges presented in fig.3. We can easily tune the frequency of these localized resonance modes inside the BG1 region by changing the upper Si layer thickness of the ridges.

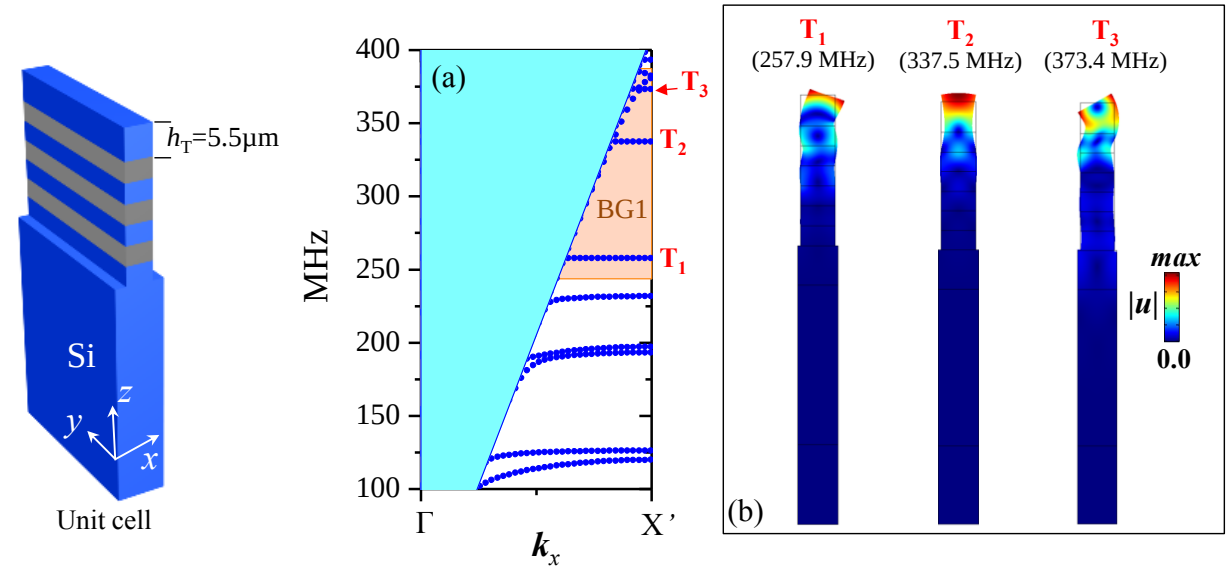

Fig.4. (a) Band structure for PC system composed of phononic ridges with thickness of the top Si layer h_T=5.5 µm. (b) Total displacement field amplitude $|u|$ for the confined modes inside the band gaps at X' point.

This time, we consider the case where we also change the thickness of the Si layer at the bottom of the ridge, denoted h_b, in contact with the substrate (fig.5(a)). Fig.5(b) shows the band structures when h_b is chosen to be 8 µm while the top Si layer thickness is h_T=5.5 µm. The other Si and W layers have their thickness fixed to 3.5 µm. We also display in fig.5(c) the total displacement field amplitude $|u|$ together with the shape of the deformation for the modes inside the band gap BG1 at X' point. In addition to the presence of the resonance modes T_1, T_2 and T_3 where the mechanical vibration is confined in the top Si/W layers, we observe the appearance of two modes denoted A and B in the band structure inside the BG1 (shaded orange region) (fig.5(b)). The displacement field maps of these modes show that they are local resonance modes with almost zero group velocity at the X' point of the first Brillouin zone. For both modes A and B, we can clearly see that the elastic energy is confined within the bottom Si/W layers close to the substrate surface, with a quickly decaying of the displacement amplitude along the upper Si/W layers and almost no vibration in the top layers of the ridge. Furthermore, when analyzing the mode's deformation shape, we can clearly see that mode A has flexural like vibrations of the ridge. The mechanical vibrational motion of mode B is mainly along z direction and corresponds to a compressional like vibration where the two bottom Si and W layers are stretched and compressed along z direction. Furthermore, one can observe in fig.5 that the defect modes T_1, T_2 and T_3 are in the same frequencies as in the case of fig.4 since these modes are not affected by the thickness change of the bottom Si layer.

We end up with an interesting feature for this system which is the existence of two families of cavity modes: one where the elastic energy is confined in the top of the phononic ridge and the other within the bottom layers in contact with the substrate. We can also have the possibility to tune the frequencies of the two kinds of modes almost independently by either varying the thickness of the upper or bottom Si layers. In the next section, we study the excitation of these modes by performing SAW transmission calculations, and investigate the coupling between the modes of interest.

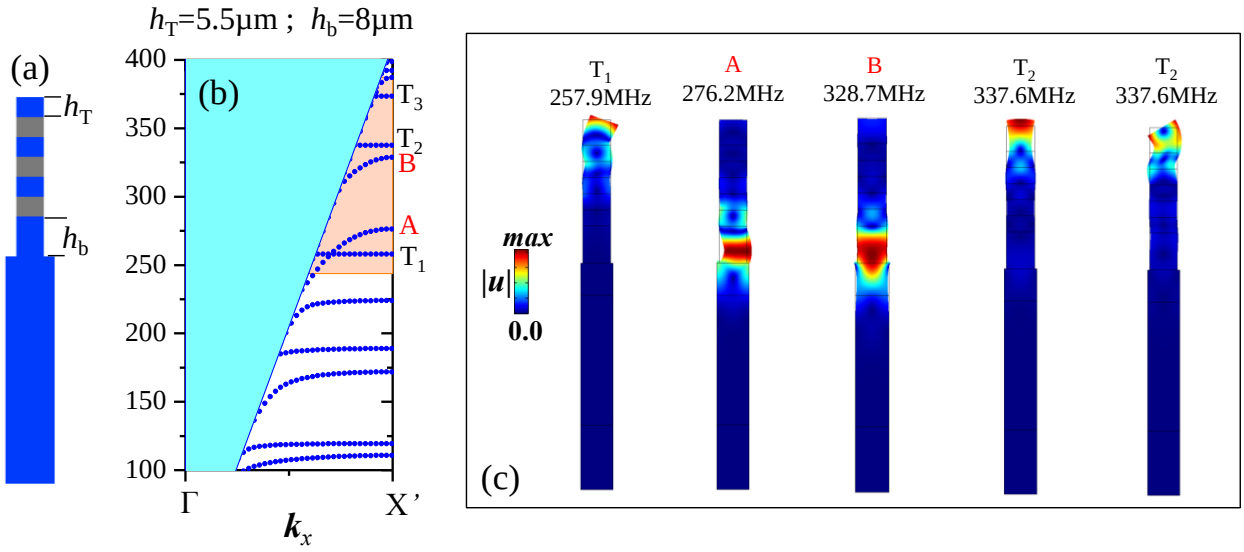

Fig.5. (a) Unit cell of the PC system where the thickness of the bottom Si layer h_b is fixed to 8 µm while the top Si layer thickness is h_T=5.5 µm. (b) Band structures for PC system. (c) Total displacement field amplitude $|u|$ for the confined modes inside the band gaps at X' point.

III. SAW transmission through a phononic ridge

In this section, we study the interaction between the SAW and a single phononic ridge by transmission calculations as schematically described in fig.6(a). Later we shall discuss the effect of a series of parallel ridges. The objective is to understand the coupling mechanisms between the surface modes, the localized modes in the bottom of the ridge and the SAW inside the BG1 region. We consider the same finite phononic ridge as the one displayed in fig.4. Fig.6(a) presents the model constructed for the transmission calculation where IDT lines footprints are used to excite the SAW at the central frequency 350MHz of the band gap BG1. Perfectly Matched Layers (PML) are applied to avoid waves reflections at the boundaries and model the infinite wave propagation into the bulk substrate. The SAW transmission coefficient is calculated by evaluating the total amplitude of the displacement field $\sqrt{|u_x|^2 + |u_z|^2}$ along the output point indicated in fig.6(a). Fig.6(b) and (c) show the transmission spectra for the cases of top layer thicknesses h_T=5.5 µm and h_T=4.7 µm respectively while the other layers

thicknesses are kept fixed to 3.5 µm. The BG1 region of the phononic ridge is shaded with orange color. For h_T=5.5 µm, we can depict the presence of three dips inside the BG1 located at frequencies 257.9, 337.5 and 373.6 MHz. At these frequencies, we plot in fig.7 the total displacement field in the phononic ridge as well as the u_z component in the substrate. We can clearly see that the dips originate from the excitation of resonance modes where the mechanical vibration is localized in the top Si/W layers of the ridge. They correspond to the resonance modes T_1, T_2 and T_3 observed in fig.4 at the same frequencies. The dips are created by the excitation of the resonance modes which couples with Rayleigh waves causing a narrow band transmission loss and part of the elastic energy radiates into the bulk substrate. More precisely, when the SAW hits the ridge, an amount of the elastic energy is transmitted through the ridge inside the BG as we consider only 3 cells. The resonance modes will be then excited in the top of the ridge. One can consider the top Si/W layers as a cavity where the elastic energy is stored at the resonance frequency and scattered back along the ridge into the substrate. This mechanism results in SAW dips (loss) in the transmission spectrum in a narrow band corresponding to the resonance modes. Also, it seems that the coupling is stronger for the flexural surface modes T_1 and T_3 where higher SAW attenuation is depicted compared to the case of the compressional mode T_2. Intuitively, the reason behind this behavior is that a ridge offers less mechanical resistance for bending than compression. This mechanical scheme makes the resonance modes T_1 and T_3 which have flexural mechanical vibration to be easily excited and coupled with SAW compared to the compressional modes T_2. Furthermore, when looking closely to the mechanical vibration amplitudes, we can notice that at the modes resonance frequency, the maximum of the displacement amplitude in the ridge is at least one order of magnitude higher than the u_z amplitude of SAW for the three dips. Additionally, an interesting feature displayed by this system is that we can easily tune the frequencies of the dips only by changing the thickness h_T of the top Si layer. When lowering the value of h_T from 5.5 to 4.7 µm (fig.6(b) and (c)), the dips frequencies can be increased inside the band gap BG1. The three dips experience high mechanical QF which is evaluated at 2.8×10^4, 1.85×10^4 and 7.2×10^3 for the three modes T_1, T_2 and T_3 respectively in fig.6(c) for instance.

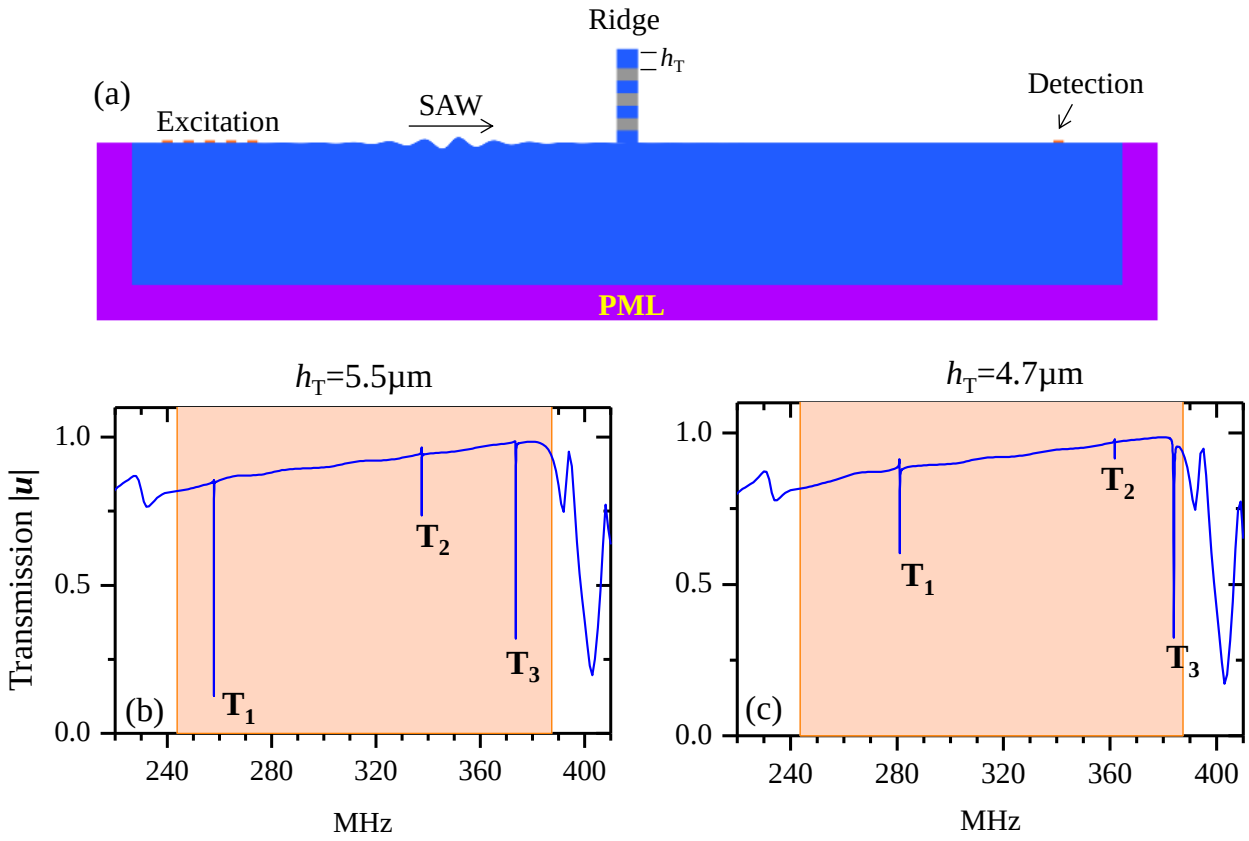

Fig.6.(a) Schematic view of the model used for the transmission calculation through one phononic ridge. (b) and (c), Transmission spectra : normalized total displacement's amplitude for h_T=5.5 µm (b) and h_T=4.7 µm (c). The shaded region indicates the phononic BG of the ridge.

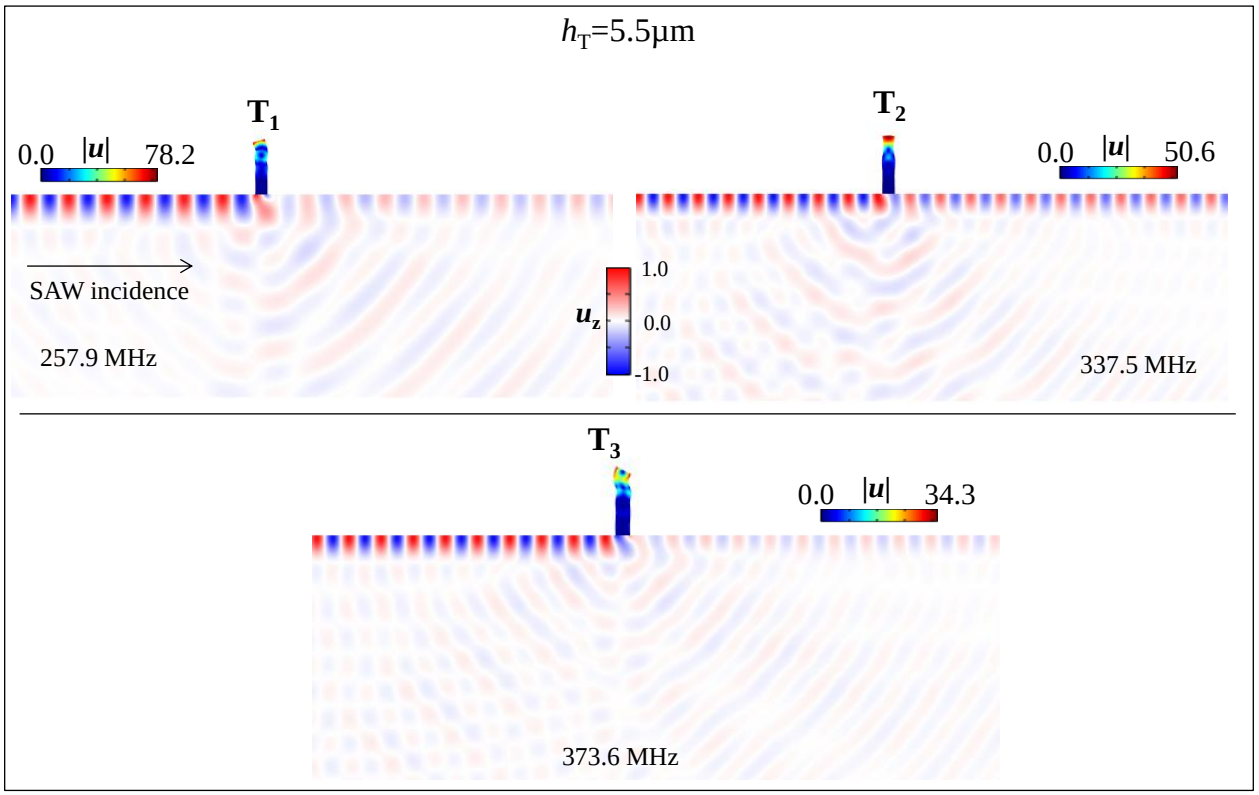

Fig.7. Total displacement field in the ridge as well as the u_z component in the Si substrate for SAW at the frequencies of the modes T_1, T_2 and T_3 indicated in fig.6 for h_T=5.5 µm.

In the following study, we calculate the transmission of SAW through one finite phononic ridge where we change the thickness of the bottom Si layer of the ridge in contact with the substrate. Fig.8(a) shows the results where h_b is fixed to 8 µm and the other layers thicknesses are kept equal to 3.5 µm in the ridge. We first observe a large attenuation band (broad dip) in the region of the band gap BG1 where the SAW transmission is around 60% between 293 and 361 MHz. Actually, this decay in the transmission is caused by the SAW excitation of the flexural mode A and the compressional mode B observed in fig.5 where the mechanical vibration is confined within the bottom Si/W layers of the ridge in contact with the substrate. More precisely the broad dip in the BG1 results from the overlapping of the two wide band dips associated with the modes A et B as we shall see more clearly when considering the transmission through a series of three ridges. Furthermore, we also notice the presence of a sharp transmission peak/dip around 342.7 MHz (zoom of the peak/dip in the right panel) in the transmission spectrum. We plot in fig.9(a), (b) and (c) the total displacement field in the ridge and the out-of-plane displacement component u_z in the substrate, respectively at 300 and 356 MHz indicated by red arrows in the attenuation band and at the peak frequency 342.7 MHz in fig.8(a). Form fig.9(a) and (b), we can observe the excitation of the flexural mode A and the compressional mode B where the strain energy is confined within the bottom layers of the

phononic ridge in contact with the substrate. Also, we can easily deduce from fig.9(c) that the peak/dip located at 342.7 MHz corresponds to the flexural resonance mode T_1 at the surface of the ridge which is at the same frequency as in the case of fig.2.

Meanwhile, we plot in fig.8(b) the transmission spectrum for the case where we increased the thickness of the Si top layer h_T to 4.5 µm while h_b is fixed to 8 µm. We observe the existence of two peaks at 288.8 MHz and 366.4 MHz where we have 96 % and 87 % of the maximum SAW transmission respectively. When analyzing the displacement field shapes of these two peaks displayed in fig.9(d) and (e), one can easily conclude that they correspond to the resonance modes T_1 and T_2 which are excited at their natural frequency as we can deduce from figure 3(c) for the chosen h_T=4.5 µm. From fig.8, we can conclude that upon increasing of the top Si layer thickness h_T, the frequencies of modes T_1 and T_2 decrease so that T_2 falls into the BG1 region when h_T=4.5µm.

In summary, we can derive an interesting feature regarding this system. First, the SAW interaction with the ridge results in the excitation of localized resonance modes where the mechanical vibration is confined within the top layers of the ridge, i.e. modes T_1, T_2 and T_3 in fig.6. These modes fall into the phononic band gap BG1 and their natural frequency can be tuned by changing the thickness of the upper Si layer h_T. The SAW interaction with the resonance modes results in a quick decay of the SAW amplitude in a very narrow bandwidth observed as sharp dips in the transmission spectrum (fig.6(b) and (c)). Meanwhile, when introducing a defect in the bottom of the phononic ridge by changing the thickness of the Si layer in contact with the substrate, we can create another kind of modes where the mechanical vibration is confined within the Si/W bottom layers of the ridge, i.e. modes A and B in fig.5(b). The excitation of these modes by SAW results in a wider bandwidth attenuation in the transmission. When the frequencies of the resonance modes T_1, T_2 of the ridge falls into the attenuation band, the transmission curve displays an asymmetric peak feature (fig.8(b)) known as Fano-like resonance [55] in the form of high SAW transmission with a very narrow band. The origin of this Fano-like behavior comes from a strong coupling between each of the resonance modes T_1 and T_2, and the confined modes A and B within the band gap region BG1. The Fano resonance was observed experimentally by Nardi et al. [56, 57] for SAW in PC where the resonance results from the coupling between surface modes and BAW. Our approach is different since Fano resonance in the proposed multilayered ridges result from the coupling between the surface modes localized on the top free surface of the ridge and the confined modes within the substrate/ridge interface.

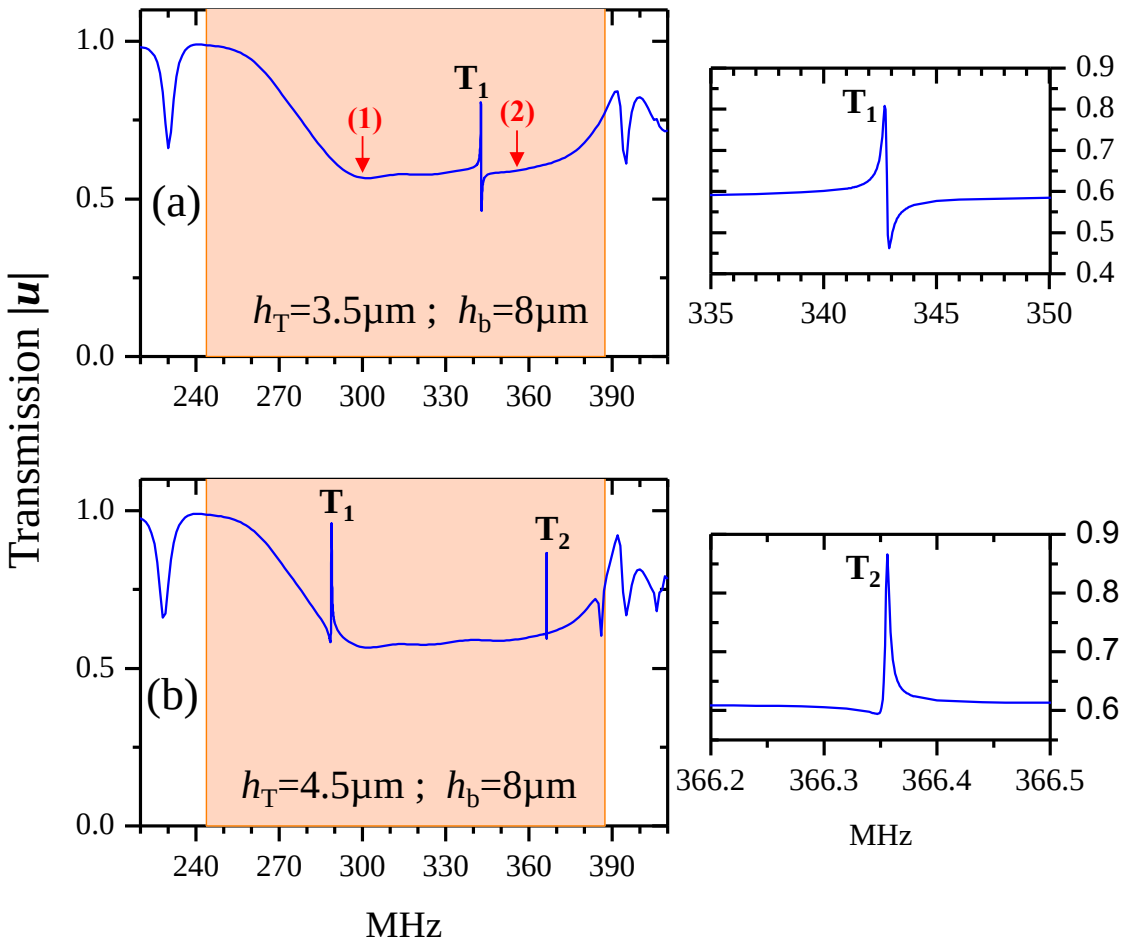

Fig.8. Transmission spectra: normalized total displacement's amplitude for h_T=3.5 µm (a) and h_T=4.5 µm (b). The bottom Si layer thickness is fixed to h_b=8 µm. The right panels are zooms of the peaks of interest for each transmission curve.

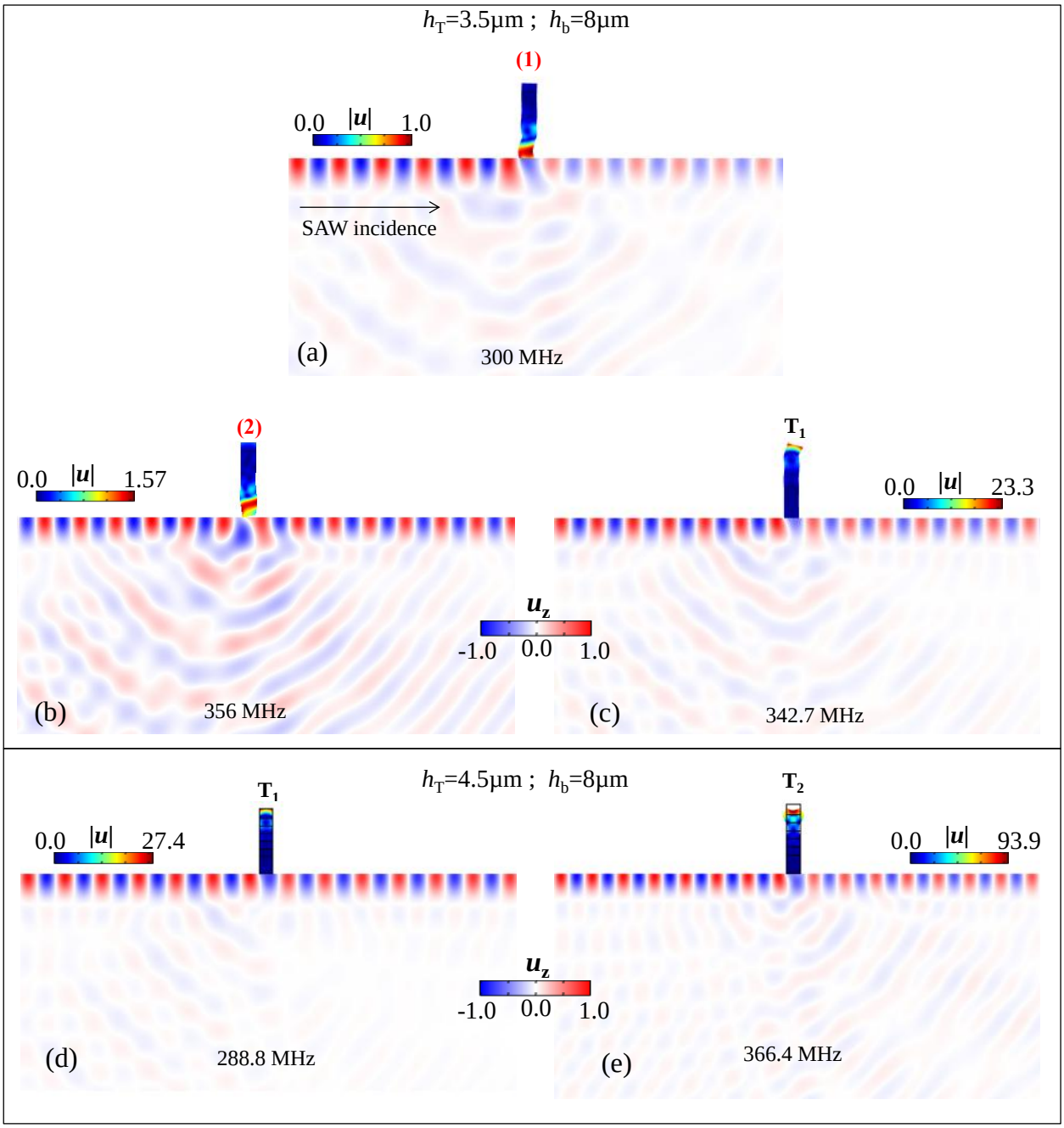

Fig.9. Total displacement field in the ridge as well as the u_z component in the Si substrate at the frequencies indicated by a red arrows (a), (b) and T_1 (c) in fig.8(a) for the case of h_T=3.5 µm. The lower panel is for the case h_T=4.5 µm at the frequencies of the peaks T_1 (d) and T_2 (e) in fig.8(b).

Finally, we calculate the SAW transmission over three phononic ridges with 21 µm distance apart to avoid interaction between the ridges. The ridges have their bottom Si layer thickness fixed to h_b=8 µm. In fig.10, we plot the transmitted SAW amplitude where the top Si layer thickness h_T is chosen to 4.25 µm (a) and 4.9 µm (b) respectively. First, we can distinguish in both transmission curves the existence of two

large attenuation bands indicated by A and B which correspond to the flexural mode and the compressional mode in which the mechanical vibrations are confined within the bottom Si/W layers of the ridges. We can clearly see the overlapping of the resonance bands of modes A and B where the transmission is at 11 % and 14 % respectively. Meanwhile, in fig.10(a), we choose the thickness h_T=4.25 µm so that the resonance mode T_1, which has flexural mechanical motion on the top Si layer, falls exactly at the attenuation region caused by the mode A. The coupling between the two modes results in a high transmission peak of 83% at the T_1 mode's frequency 300 MHz. Both modes have the same mechanical motion nature, i.e. flexural vibration, which explains their strong coupling. The total displacement field amplitude in the ridges and the u_z component in the substrate plotted in the lower panel of fig.10(a), shows the excitation of the resonant mode T_1 in the three ridges by the SAW at the peak frequency 300 MHz along with the transmitted SAW. We can also have the same behavior in the attenuation band B by coupling this mode with the resonance mode T_2 knowing that they both have the same mechanical motion nature, i.e. compressional vibration. In fact, by choosing Si top layer thickness h_T=4.9 µm, the frequency of the compressional mode T_2 can be tuned to fall into the attenuation band B where the coupling between the modes results in the creation of the peak T_2 depicted in fig.10(b). At the frequency 356.5 MHz of the peak T_2, a maximum transmission of 66% is reached for SAW. When analyzing the total displacement field amplitude in the ridges and the u_z component in the substrate plotted in the lower panel of fig.10(b) we can clearly see the excitation of the resonant mode T_2 in the three ridges by the SAW. The QF of mode T_1 is about 1200 in the case of h_T=4.25µm (fig.10(a)) while the QF of mode T2 is 2.89×10^4 in the case of h_T=4.9µm (fig.10(b)). Moreover, for the two cases where either the resonance mode T_1 falls into the dip band A or mode T_2 falls into the band B, we have a situation very close to an acoustic analogue of the electromagnetically induced transparency (EIT) [58,59]. In fact, in plasmonic crystals for instance, the coupling between localized surface states (known as Tamm states) and the defect plasmonic state give an EIT-like behavior [60].

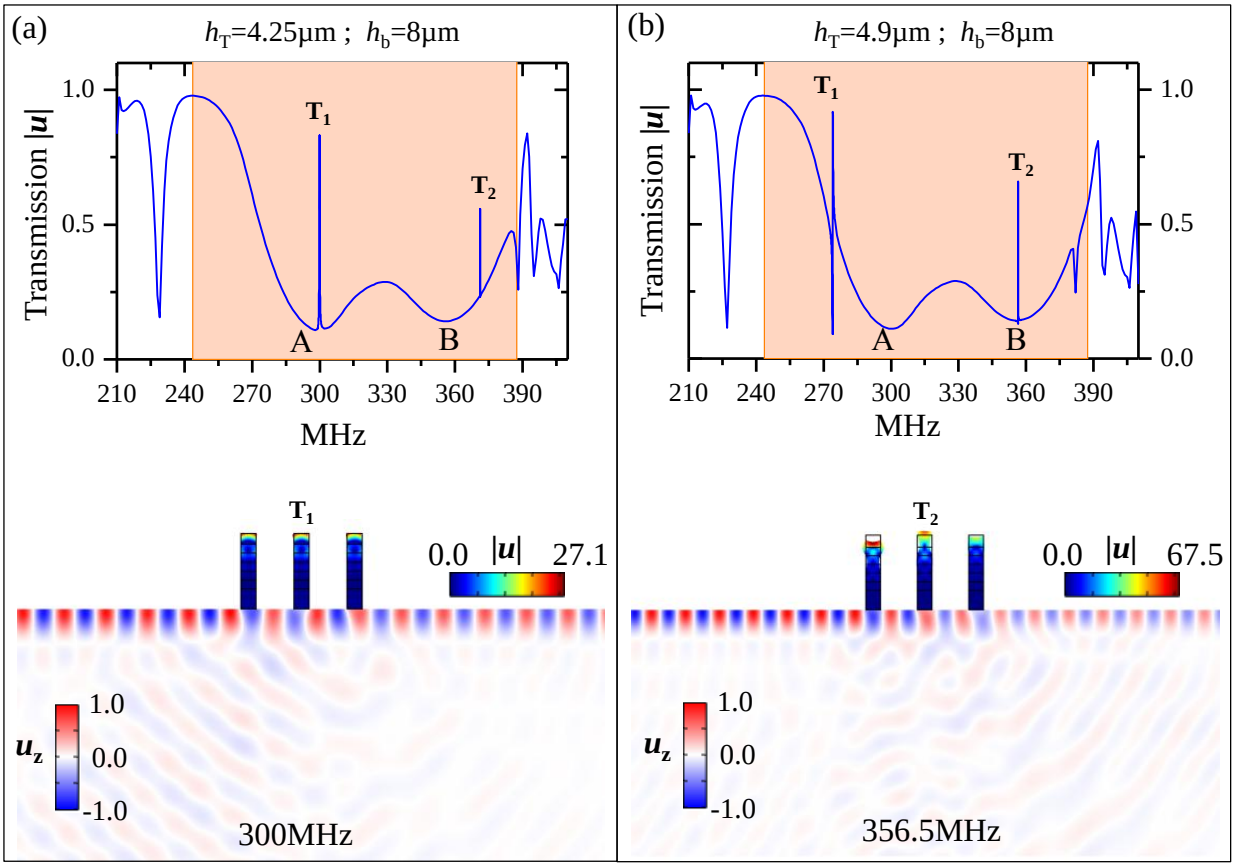

Fig.10. Transmission results: normalized total displacement's amplitude for h_T=4.25 µm (a) and h_T=4.9 µm (b). The bottom Si layer thickness is fixed to h_b=8 µm. (Bottom panels) Total displacement field in the ridge as well as the u_z component in the Si substrate for SAW at T_1 for the case h_T=4.25 µm (a) and T_2 for the case h_T=4.9 µm (b).

Conclusion

The SAW dispersion over a periodic repetition of periodic multilayered ridges undergoes interesting properties for efficient SAW manipulation. The phononic BG of the ridge allows the existence of resonance modes localized within the first phononic layers at the free end of the ridge. The SAW interaction with these modes results in a sharp decay of the SAW amplitude in the form of high QF dips. Moreover, another family of confined modes can be created inside the band gap where the elastic energy is confined within the first layers of the ridge in contact with the substrate surface. The excitation of these modes by SAW causes a broad decay of the SAW amplitude in a relatively wide band. The high QF confined modes in the upper free edge of the ridge can couple with the localized modes in ridge/substrate interface to give rise to Fano like resonance with high QF SAW transmission peaks. This result is a very interesting achievement in the sense that the phononic ridge based PC can be proposed for efficient manipulation of SAW with low leakage into the substrate. The structure can introduce a new approach for using PC in SAW based devices to increase the performance of sensing for instance. Meanwhile, the high

transmission peak created by coupling the localized surface modes and the modes confined within the ridge/substrate interface tends towards the arising of an acoustic analogue of the electromagnetically induced transparency (EIT). Moreover, a phononic ridge can be used to excite high QF surface phonons which can then couple with external photons. Very recently, Anguiano et al. [61] and Lamberti et al. [62] demonstrated the confinement of both phonons and photons with a strong optomechanic coupling in a composite multilayered GaAs/AlAs micopillar. The composite pillar based system would be a promising structure to observe quantum optomechanic phenomena, and even to be integrated into a biosensing platform for instance to increase the device sensitivity. For a practical application in biosensing, the top free surface of the ridge can be functionalized with antigens where specific antibodies can be covalently grafted. The molecular binding event can then be monitored through a real time observation of the mechanical frequency shift of the localized modes in the SAW spectrum. Meanwhile, the multilayered ridge system can also be used for macroscale application in the frame of earthquake damage control for instance. One can imagine an appropriate design of periodically structured ridges so that their transmission spectrum can be tuned to scatter the earthquake surface wave into the bulk [63]. Finally, one can also tailor a defect inside the phononic ridge or pillar to create other cavity modes and achieve the same previous properties to obtain high QF SAW transmission peaks.

References

[1] M. S. Kushwaha, P. Halevi, L. Dobrzynski, and B. Djafari-Rouhani, Phys. Rev. Lett **71**, 2022 (1993).

[2] M. Sigalas and E. N. Economou, Solid State Communications, **86**, 141 (1993).

[3] M. Kafesaki, M. M. Sigalas, and N. Garcia, Phys. Rev. Lett. **85**, 4044 (2000).

[4] C. Qiu, Z. Liu, J. Mei, and J. Shi, Appl. Phys. Lett. **87**, 104101 (2005).

[5] T. T.Wu, L. C.Wu, and Z. G. Huang, J. Appl. Phys. **97**, 094916 (2005).

[6] J. O. Vasseur, P. A. Deymier, B. Djafari-Rouhani, Y. Pennec, and A-C. Hladky-Hennion. Phys. Rev. B **77**, 085415 (2008)

[7] Y. Pennec, B. Djafari Rouhani, H. Larabi, A. Akjouj, J. N. Gillet, J. O. Vasseur, and G. Thabet, Phys. Rev. B **80**, 144302 (2009)

[8] J.-H. Sun and T.-T. Wu, Phys. Rev. B **74**, 174305 (2006)

[9] Y. Pennec, B. Djafari-Rouhani, J. O. Vasseur, A. Khelif, P. A. Deymier, Phys.Rev. E **69**, 046608 (2004)

[10] S. Amoudache, R. Moiseyenko, Y. Pennec, B. Djafari-Rouhani, A. Khater, R. Lucklum, and R. Tigrine, J. Appl. Phys. **119**, 114502 (2016)

[11] T.-T. Wu, Y.-T. Chen, J.-H. Sun, Sz.-C. Steven Lin, and T. J. Huang , Appl. Phys. Lett. **98**, 171911 (2011)

[12] J. Zhao, B. Bonello, L. Becerra, O. Boyko, and R. Marchal. Appl. Phys. Lett. **108**, 221905 (2016)

[13] J. Zhao, B. Bonello, R. Marchal, and O. Boyko, New J. Phys. **16**, 063031 (2014).

[14] S.-C. S. Lin, T. J. Huang, J.-H. Sun, and T.-T.Wu, Phys. Rev. B **79**, 094302 (2009).

[15] L.-H. Wu and X. Hu, Phys. Rev. Lett. **114**, 223901 (2015)

[16] C. He, X. Ni, H. Ge, X.-C. Sun, Y.-B. Chen, M.-H. Lu, X.-P. Liu, and Y.-F. Chen, Nature Physics **12**, 1124 (2016)

[17] Z. Liu, X. Zhang, Y. Mao, Y. Y. Zhu, Zh. Yang, C. T. Chan, and Ping Sheng. Science **289**, 1734 (2000)

[18] J. Li and C. T. Chan, Phys. Rev. E **70**, 055602 (R) (2004)

[19] Y. Ding, Z. Liu, C. Qiu, and J. Shi, Phys. Rev. Lett. **99**, 093904 (2007)

[20] M. Oudich, B. Djafari-Rouhani, Y. Pennec, M. B. Assouar, and B. Bonello, J. Appl. Phys. **116**, 184504 (2014).

[21] J. Mei, G. Ma, M. Yang, Z. Yang, W. Wen, and Ping Sheng, Nat. Comm. **3**, 756 (2012)

[22] X. Zhou, M. B. Assouar, and M. Oudich. J. Appl. Phy. **116**, 194501 (2014)

[23] X. Zhou, M. B. Assouar, and M. Oudich, Appl. Phys. Lett. **105**, 233506 (2014)

[24] M. Farhat, S. Enoch, S. Guenneau, and A. B. Movchan, Phys. Rev. Lett. **101**, 134501 (2008)

[25] A. Khelif, B. Aoubiza, S. Mohammadi, A. Adibi, and V. Laude, Phys. Rev. E **74**, 046610 (2006)

[26] J. O. Vasseur, A.-C. Hladky-Hennion, B. Djafari-Rouhani, F. Duval, B. Dubus, and Y. PennecP. A. Deymier, Appl. Phys. Lett. **101**, 114904 (2007)

[27] Y. Pennec, B. Djafari-Rouhani, H. Larabi, J. O. Vasseur, and A. C. Hladky-Hennion, Phys. Rev. B **78,** 104105 (2008)

[28] T.-T. Wu, Z.-G. Huang, T.-C. Tsai, and T.-C. Wu, Appl. Phys. Lett. **93**, 111902 (2008).

[29] T.-C. Wu, T.-T. Wu, and J.-C. Hsu, Phys. Rev. B **79,** 104306 (2009)

[30] M. Oudich, Y. Li, B. M. Assouar, and Z. Hou, New J. Phys. **12**, 083049 (2010)

[31] M. B Assouar, and M Oudich, Appl. Phys. Lett. **100**, 123506 (2012)

[32] M. Oudich, M. Senesi, M. B. Assouar, M. Ruzzene, J.-H. Sun, B. Vincent, Z. Hou, and T.-T. Wu. Phys. Rev. B **84**, 165136 (2011)

[33] M. Oudich, X. Zhou, and M. B. Assouar, J. Appl. Phys. **116**, 193509 (2014)

[34] B. Assouar, M. Oudich, X. Zhou, Comptes Rendus Physique, **17**, 524 (2016)

[35] Y. Jin, N. Fernez, Y. Pennec, B. Bonello, R. P. Moiseyenko, S. Hémon, Y. Pan, and B. Djafari-Rouhani, Phys. Rev. B **93**, 054109 (2016)

[36] Y. Jin, E. H. EI Boudouti, Y. Pennec, and B. Djafari-Rouhani, J. Phys. D: Appl. Phys. **50**, 425304 (2017)

[37] Y. Jin, Y. Pennec, Y. Pan and B. Djafari-Rouhani, Crystals **6**, 64 (2016)

[38] T.-T. Wang, Y.-F. Wang, Y.-S. Wang, and V. Laude, Appl. Phys. Lett. **111**, 041906 (2017)

[39] Y. Jin, B. Bonello, R. P. Moiseyenko, Y. Pennec, O. Boyko and B. Djafari-Rouhani, Phys. Rev. B **96**, 104311 (2017)

[40] M. B. Assouar, M. Senesi, M. Oudich, M. Ruzzene, and Z. Hou, Appl. Phys. Lett. **101**, 173505 (2012)

[41] P. Celli and S. Gonella, Appl. Phys. Lett **107**, 081901 (2015)

[42] M. Oudich, and Y. Li, J. Phys. D: Appl. Phys. **50**, 315104 (2017)

[43] T. T. Wu, Z. G. Huang, and S. Lin, Phys. Rev. B **69**, 094301 (2004).

[44] V. Laude, M. Wilm, S. Benchabane, and A. Khelif, Phys. Rev. E, **71**, 036607, (2005)

[45] S. Benchabane, O. Gaiffe, G. Ulliac, R. Salut, Y. Achaoui, and V. Laude, Appl. Phys. Lett. **98,** 171908 (2011)

[46] D. Yudistira, Y. Pennec, B. Djafari Rouhani, S. Dupont, and V. Laude. Appl. Phys. Lett. **100**, 061912 (2012)

[47] A. Khelif, Y. Achaoui, S. Benchabane, V. Laude, and B. Aoubiza, Phys. Rev. B **81**, 214303 (2010).

[48] Y. Achaoui, A. Khelif, S. Benchabane, L. Robert, and V. Laude, Phys. Rev. B **83**, 104201 (2011)

[49] J. F. Robillard, A. Devos, and I. Roch-Jeune, Phys. Rev. B **76**, 092301 (2007)

[50] C. Giannetti, B. Revaz, F. Banfi, M. Montagnese, G. Ferrini, F. Cilento, S. Maccalli, P. Vavassori, G. Oliviero, E. Bontempi, L. E. Depero, V. Metlushko, and F. Parmigiani, Phys. Rev. B **76**, 125413 (2007)

[51] D. Yudistira, A. Boes, B. Graczykowski, F. Alzina, L. Y. Yeo, C. M. Sotomayor Torres, and A. Mitchell, Phys. Rev. B **94**, 094304 (2016)

[52] B. J. Ash, S. R. Worsfold, P. Vukusic, and G. R. Nash, Nature Communications **8**, 174 (2017)

[53] M. A. Al Lethawe, M. Addouche, S. Benchabane, Vincent Laude, and Abdelkrim Khelif, AIP Advances **6**, 121708 (2016)

[54] S. Benchabane, R. Salut, O. Gaiffe, V. Soumann, M. Addouche, V. Laude, and A. Khelif Phys. Rev. B **8**, 034016 (2017)

[55] U. Fano, Phys. Rev. **124**, 1866 (1961)

[56] D. Nardi, M. Travagliati, M. E. Siemens, Q. Li, M. M. Murnane, H. C. Kapteyn, G. Ferrini, F. Parmigiani, and F. Banfi, Nano Lett. **11**, 4126 (2011),

[57] D. Nardi, M. Travagliati, M. M. Murnane, H. C. Kapteyn, G. Ferrini, C. Giannetti, and Francesco Banfi, Sensors Journal IEEE **15**, 5142 (2015).

[58] K.-J. Boller, A. Imamoglu, and S. E. Harris, Phys. Rev. Lett. **66**, 2593 (1991)

[59] M. Fleischhauer, A. Imamoglu, and J. P. Marangos, Rev. Mod. Phys. **77**, 633 (2005)

[60] G. C. Dyer, G. R. Aizin, S. J. Allen, A. D. Grine, D. Bethke, J. L. Reno, and E. A. Shaner, Nature Photonics **7**, 925 (2013)

[61] S. Anguiano, A. E. Bruchhausen, B. Jusserand, I. Favero, F. R. Lamberti, L. Lanco, I. Sagnes, A. Lemaître, N. D. Lanzillotti-Kimura, P. Senellart, and A. Fainstein, Phys. Rev. Lett. **118**, 263901 (2017)

[62] F. R. Lamberti, Q. Yao, L. Lanco, D. T. Nguyen, M. Esmann, A. Fainstein, P. Sesin, S. Anguiano, V. Villafañe, A. Bruchhausen, P. Senellart, I. Favero, and N. D. Lanzillotti-Kimura, Optics Express **25**, 24437 (2017)

[63] A. Colombi, P. Roux, S. Guenneau, P. Gueguen, and R. V. Craster, Scientific Reports **6**, 19238 (2016)